Z. Phys. A 356, 299–308 (1996)

ZEITSCHRIFT
FÜR PHYSIK A

High-energy gamma-rays accompanying the spontaneous fission of ^{252}Cf

A. Hotzel[1,2,⋆], P. Thirolf[1,2,⋆⋆], Ch. Ender[1,2], D. Schwalm[1,2], M. Mutterer[3], P. Singer[3], M. Klemens[3], J. P. Theobald[3,⋆⋆⋆], M. Hesse[4], F. Gönnenwein[4], H. v. d. Ploeg[5]

[1] Max-Planck-Institut für Kernphysik, D-69117 Heidelberg, Germany
[2] Physikalisches Institut, Universität Heidelberg, D-69120 Heidelberg, Germany
[3] Institut für Kernphysik, Technische Hochschule Darmstadt, D-64289 Darmstadt, Germany
[4] Physikalisches Institut der Universität Tübingen, D-72076 Tübingen, Germany
[5] Institut de Physique Nucleaire, F-91406 Orsay Cedex, France

Received: 19 July 1996
Communicated by B. Povh

Abstract. The γ-ray spectrum of ^{252}Cf(sf) was measured in the Darmstadt-Heidelberg Crystal Ball spectrometer, with a double ionization chamber mounted inside to detect the fission fragments. The measurement was aimed at a better understanding of an unusual component found in the high-energy region between 3 and 8 MeV, with fragment mass splits near symmetry. This component was proved to be predominantly emitted by the heavier fragment, to reach its highest intensity at a fragment mass split of 132:120, and to have an almost isotropic angular distribution. Calculations with the statistical code CASCADE could reproduce the main features.

PACS: 25.85.Ca

1 Introduction

In a fission reaction, the majority of γ-rays are emitted by the excited fragments after the end of neutron evaporation. They fall into two categories, commonly called the statistical and the discrete γ-rays. The statistical γ-rays originate mainly from electric dipole transitions, and carry away most of the remaining excitation energy of the fragments. Their energy spectrum is of the form $Y(E_\gamma) \propto {E_\gamma}^x \cdot \exp\left(-E_\gamma/(kT)\right)$, with $3 \leq x \leq 4$. The discrete γ-rays originate mainly from electric quadrupole transitions along the yrast sequence of the fragments; they carry away most of the angular momentum of the fragments. They lead to an enhancement of the γ-energy spectrum in the region below 1.5 MeV. Thus the γ-energy spectrum observed in a fission reaction shows an exponential decrease above 1.5 MeV which continues up to energies greater than 8 MeV, where the onset of the GDR again leads to an enhancement of the spectrum.

In 1988, a striking exception to this general trend was found in the spontaneous fission of ^{252}Cf [1]. There, fission events with fragment mass splits near symmetry show a γ-energy spectrum with a pronounced bump between 3 and 8 MeV, which will be referred to as the "high-energy component" or simply as the "γ-bump" in the present article. In a later experiment [2] the intensity of the γ-bump was found to be maximal for mass splits around 120:132 rather than for symmetric fission. In order to gain further information on the mass dependence, heavy-ion induced fission reactions with different compound nuclei were studied [3]. In all studied reactions a bump in the γ-spectrum was found for fragment masses around 132, while the masses of the complementary fragments varied according to the mass of the compound nucleus. Moreover, the mass distributions of the γ-bump showed widths which were strongly correlated to the N/Z ratio of the compound nuclei. These findings pointed to the shell closures at Z=50 and N=82 as the cause of the high-energy component. On the theoretical side, the strong mass dependence of the γ-bump has triggered several suggestions as to the origin of this rather intense high-energy γ-component. Glässel et al. [1] and later Brosa et al. [4] suggested that these γ-rays might be emitted in the contraction of the nascent fission fragments connected with the so-called "superlong" fission channel, which mainly leads to symmetric fission and results in very strongly deformed fragments. Pomorski et al. [5] speculated that the enhancement might result from large amplitude vibrations excited in the fission products during the scission process. On the other hand, Hofman et al. [6] claimed that the observed enhancement of the γ-spectra could be understood within the statistical model by taking into account the different fragmentation energies, although the agreement between the calculated and the measured spectra was rather poor.

In order to get more detailed experimental information on the γ-bump and its possible origin, an improved experiment on the properties of these γ-rays in the spontaneous fission of ^{252}Cf seemed desirable.

2 Experimental method

The experimental setup consisted of two 4π-detectors, a double ionization chamber to detect the fission fragments and

⋆ *Present address*: Fritz-Haber-Institut der MPG, D-14195 Berlin, Germany
⋆⋆ *Present address*: Beschleunigerlabor der Ludwig-Maximilian-Universität München, D-85748 Garching, Germany
⋆⋆⋆ Deceased

the Darmstadt-Heidelberg Crystal Ball. The crystal ball spectrometer has been described in detail elsewhere [7]; it is a 4π-detector made of 162 NaI-scintillator crystals, which form a sphere with an inner diameter of 50 cm. The crystal ball served as γ-ray detector with high efficiency and angular resolution.

2.1 The double ionization chamber

For the detection of the fission fragments, a double ionization chamber (DIC) was built into the crystal ball. The outer wall of the DIC was made of 1 mm aluminum and had an almost spherical shape with a diameter of 30 cm. It was filled with methane at 570 torr.

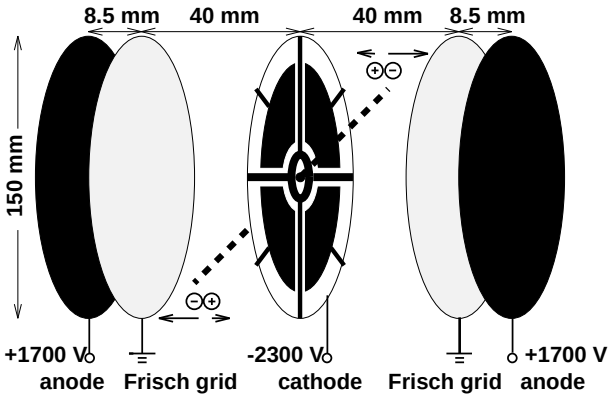

Fig. 1. Inner setup of the DIC. Conducting areas are black. The thin ^{252}Cf source was mounted in the hole in the center of the cathode

Figure 1 shows a sketch of the inner setup of the DIC. It consisted of 5 round disks with a diameter of 15 cm mounted on ceramical rods. The middle disk was the cathode, to each side of which a Frisch grid and an anode plate were mounted. The cathode consisted of a printed circuit board of 1.6 mm thickness with a central hole of 16 mm diameter. The two sides of the cathode were subdivided into four quadrants and a central ring each; while the 8 quadrants were read out individually, the two rings were connected and processed together. The ^{252}Cf source had a diameter of 5 mm and a fission activity of 400/s. It was mounted on a thin backing (30 μg/cm^2 Al_2O_3, with 10 μg/cm^2 Au evaporated onto both sides) in the hole in the center of the cathode and was electrically connected to the central ring. The whole setup was reflection symmetric to the cathode plane and, with the exception of the segmented cathode, axially symmetric.

The operating principle of the chamber is as follows: At fission, the two fragments recoil with roughly 4% of the speed of light into the two opposite hemispheres. The kinetic energies of the fragments are converted into ionization energy, and the fragments stop before reaching the Frisch grids. The free electrons start drifting towards the anodes and induce the common "start" signal in the central sector of the cathode. The anode time signals are caused by the first electrons which pass the Frisch grids and are thus linearly dependent on both the lengths of the fragment tracks and the cosine of the polar angle θ. The anode energy signals are proportional to the number of electrons produced during the deceleration of the fragments and thus proportional to their kinetic energies. From momentum conservation, the ratio of the primary fragment masses is inversely equal to the ratio of the kinetic energies. However, the measured kinetic energies are reduced and smeared out by neutron evaporation. The correction for this effect was carried out with data tables listing the mean neutron multiplicity as a function of fragment mass and total kinetic energy (TKE) [8]. Throughout this article, the mass values A refer to the fragments before neutron evaporation, unless otherwise stated. The TKE values refer to the fragments *after* neutron evaporation.

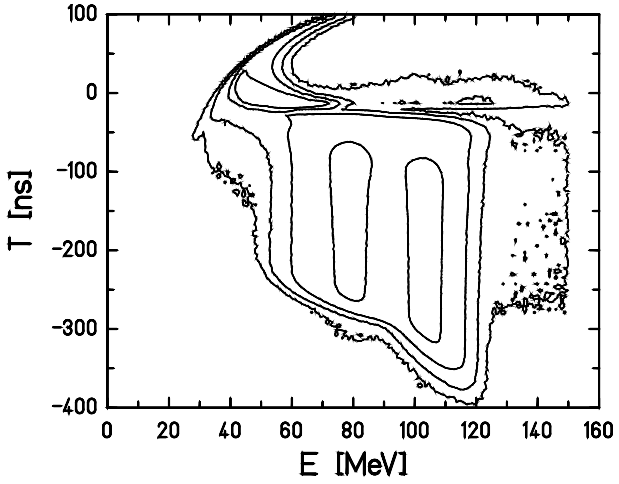

Fig. 2. Energy–time spectrum of one anode (see text). The origin of the time scale is arbitrary. Logarithmic contour lines (powers of 10)

Figure 2 shows the energy–time spectrum of the anode on the backing side (this term refers to the backing of the ^{252}Cf source, as opposed to the source side). For the energy calibration, time cuts were set in the two-dimensional spectrum, and the maxima of the resulting energy distributions were identified with the most probable kinetic energy values of the heavier and the lighter fragment, taken from the literature [9]. With these data points, a linear energy calibration was performed, where the two calibration parameters were allowed to be functions of the anode time T.

The two parallel ridges in Fig. 2 correspond to the most probable kinetic energies of the heavier and the lighter fragment, the latter having the higher energy. The bottom edge of the spectrum (large negative anode times) is formed by events with fission axes in the direction of the symmetry axis, i. e. $\theta = 0°$. Its energy dependence reflects the fact that lighter fragments with higher kinetic energies have longer tracks. The top edge is formed by events with $\theta \approx 75°$. At this angle, scattering on the cathode sets in (on the source side, there is practically no scattering up to $\theta = 90°$, because the thin source was mounted in the plane formed by the source side of the cathode). The scattered particles suffer energy losses and their tracks are shortened, so that these events are accumulated in the upper left corner of the energy–time spectrum.

For the θ-calibration, a linear dependence betweeen the anode time and $\cos\theta$ was assumed. The (energy dependent)

time values for θ = 0° and θ = 90° were obtained directly from the spectra (the time values for θ = 90° could be deduced on the source side only; the values for the backing side were extrapolated).

Thus not only the two fragment energies, but also the polar angle of the fission axis could be determined from the anode signals. For the determination of the azimuthal angle ϕ of the fission axis, the four outer sectors on each side of the cathode were used.

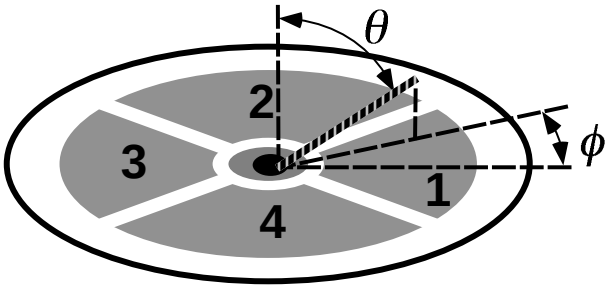

Fig. 3. Determination of the fission axis from the cathode signals

The principle of the angle determination with the cathode is sketched in Fig. 3: The energy signals of the outer sectors depend on the orientation of the fission axis, i. e. on θ and ϕ, and also on the kinetic energy of the fragment. From the heights of the signals S_i of the cathode sections i (i =1, ..., 8), the quantities q_{13} and q_{24} for the backing side, as well as q_{57} and q_{68} for the source side of the DIC are calculated, which are defined by e. g.

$$q_{13} = \frac{S_1}{S_1 + S_3} \tag{1}$$

where the sectors 1 and 3 lie on the same surface of the cathode, but opposite to each other; the other quantities are defined accordingly. The four quantities q_{ij} depend not only on the orientation θ, ϕ of the fission axis, but also on the lateral position of the fissioning nucleus in the extended ^{252}Cf source. However, since the effect of the latter on the "source side" quantities q_{57}, q_{68} is opposite to its effect on the "backing side" signals q_{13}, q_{24}, this influence can be minimized by an appropriate averaging procedure of the four quantities. Using furthermore a calibration procedure based on specific θ-values determined via the anode signals and by exploiting the cathode symmetries and the isotropic distribution of fission directions, the azimuthal angle ϕ is obtained, as well as an independent value for the polar angle θ (for more details see [10]). For small θ, the θ-values given by the cathode are more accurate than the ones taken from the anodes. In the final analysis a weighted average of the two θ-values was used.

Because of the scattering of the fragments on the backing side of the cathode, a θ-cutoff was introduced. Only events with $\theta \leq 66°$ were accepted, which still corresponds to a solid angle of $0.6 \cdot 4\pi$. Within this solid angle, the fission direction is determined with a resolution better than 12° (fwhm). This has to be compared to the opening angle of 18° of an individual NaI crystal, which determines the accuracy with which the direction of a γ-quant can be measured.

The coincidence of a signal from the central cathode sector (where the threshold was set above the signal amplitudes caused by α-decays) with at least one signal from the crystal ball was required as a trigger. The main measurement lasted 5 days, with an average event rate of 240/s. After the introduction of all cuts, $3.13 \cdot 10^7$ "good" events remained.

2.2 Mass and TKE spectra

Figure 4a shows the measured fragment mass – total kinetic energy (TKE) distribution. The mean value and the variance of the TKE show the well-known fragment mass dependence [8, 9]. As overall TKE cuts seemed inappropriate to investigate the TKE dependence of the γ-spectrum, we introduced fragment mass dependent TKE cuts: The mass–TKE plane was divided into 4 regions, as seen in figure 4a. The boundaries correspond to the mean TKE (central boundary), $\pm$fwhm$/2$ (upper and lower boundary) as functions of fragment mass. The fwhm of the TKE distribution was calculated with the formula

$$\text{fwhm} = \sqrt{8 \cdot \ln 2} \cdot \Delta \tag{2}$$

where Δ^2 is the variance of the distribution.

The TKE regions were numbered 1 to 4 with increasing TKE. All TKE cuts in this work refer to these regions.

Figure 4b shows the measured mass distribution. The mass variable A_b refers to the fragment detected on the backing side of the DIC. Here – and whenever statistics permitted – mass symmetry of the spectra was not imposed but used as a test for the symmetry of the experimental procedure. The measured mass spectrum has a peak-to-valley ratio of 25. Mass and TKE spectra are in very good agreement with previous measurements [8, 9].

The mass resolution was determined experimentally with the help of the fission product ^{134}Te, in which an isomeric state is populated which decays via a 3γ-cascade with a halflife of 160 ns [11]. Figure 4c shows the fragment mass spectrum gated on the ^{134}Te-lines taken with a delay time of $\geq$ 100 ns (after background subtraction). The peaks occur at A_b values of 135 and 252-135=117, i. e. they are shifted by 1 mass unit, which agrees well with the average evaporation of 1.2 neutrons preceding the formation of ^{134}Te [12]. The widths of the two peaks yield a fragment mass resolution of 5.0 (fwhm).

The finite mass resolution is caused by two effects, which are of the same order of magnitude. One is due to the energy resolution of the DIC, the other due to the neutron evaporation. With an estimate for the latter contribution, the TKE resolution could be deduced from the mass resolution. The resulting relative value is 4% (fwhm).

The mass resolution itself is TKE-dependent. Its fwhm decreases from 6.1 to 4.2 when going from region 1 to region 4, as was determined with the help of the ^{134}Te lines. The improvement with increasing TKE is expected as the mean neutron multiplicity decreases.

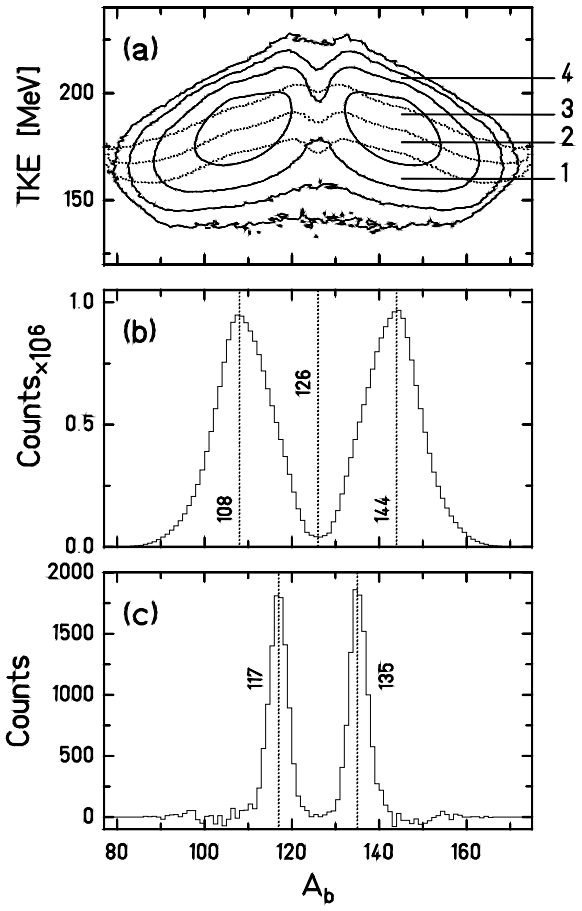

Fig. 4. a Fragment mass–TKE distribution. The dotted lines are the boundaries of the TKE regions labelled 1 to 4 (see also text; logarithmic contour lines - powers of 10). **b** Fragment mass distribution (all TKE). **c** Mass spectrum, gated on individual ^{134}Te-lines from the decay of an 160 ns-isomer. The mass variable refers to the fragment detected on the backing side of the DIC

2.3 Analysis of the crystal ball data

The NaI-detectors were calibrated with various γ-sources, and with the aid of the two inelastic scattering reactions ^{12}C(p,p')^{12}C* and ^{16}O(p,p')^{16}O*, using standard procedures. The neutron signals were clearly separated from the γ-ray signals by time-of-flight. However, serious problems were caused by γ–neutron summing, i. e. by double hits of the NaI-detectors by γ-quants and neutrons from the same fission event. In this case, the energy signal of the detector corresponds to the sum of the γ and the neutron energy, while the time signal may still be in the "prompt" region, indicating a γ-event. Despite the large granularity of the crystal ball, this effect was quite strong for γ-energies above 4 MeV, and at 7 MeV, 70% of the raw γ-spectrum were summing events. Moreover, it dominated the angular distribution at higher γ-energies, as the neutrons are strongly focussed in the direction of the fission axis. Individual summing events could not be discriminated. Therefore, the measured γ-spectra had to be corrected for this effect by an iterative folding procedure. This was complicated by the fact that whenever the neutron arrives within the CFT delay time of 50 ns and deposits a sufficient amount of energy, the NaI time signal is pushed out of the prompt region and therefore does not contribute to the measured γ-spectra (for a detailed discussion see [13, 14]).Thus the parameters of the summing correction had to be chosen carefully. In particular, the exact choice of parameters was crucial for the angular distribution of the corrected spectra, whereas it had only a weak influence on the energy spectra, and particularly on the differences of the energy spectra for different fragment mass splits.

The spectra were also corrected for γ–γ-summing. However, the influence of the γ-γ-summing on the form of the spectra was small.

A global correction for the absolute detection efficiency was not generally performed, because the deconvolution procedure can introduce systematic errors in domains of weak statistics. Some selected deconvoluted spectra will be shown in Sect. 4. Since the absolute efficiency is a smooth function of the γ-energy, and the same for all kinds of fission events, it can be neglected in the direct comparison of γ-spectra. For comparison with calculated spectra, however, the measured γ-spectra had to be deconvoluted with the response matrix of the crystal ball. This matrix was created by a GEANT simulation of the bare crystal ball und renormalized according to the full energy peak efficiencies of the actual experiment, which were taken from the calibration measurements. Moreover, the differences in efficiency between the individual γ-detectors had to be removed in order to determine the angular distribution. The relative efficiencies were directly deduced from the data of the main experiment. This was possible because the DIC covered practically 100% of the total solid angle when requiring only one correctly detected fragment; only events with fission axes lying very close to the cathode plane were lost. Thus the total ensemble of the recorded events represents an isotropic distribution of fission axes and thus of γ-rays. From this, the relative detector efficiencies were determined, which in turn yielded the relative detection efficiency as a function of γ-energy, and of the angle with the fission axis. The relative efficiency correction was carried out after the summing corrections had been made.

3 Experimental results

3.1 Fragment mass dependence and spectral shape of the high-energy component

Figure 5 shows γ-energy spectra observed for different fragment mass splits. The spectra were normalized according to the number of fissions recorded with the respective mass split. The mass values A_b at the right-hand side of the spectra refer to the fragment masses measured on the backing side of the cathode. Spectra of complementary mass splits are placed side by side. The requirement of fragment mass symmetry is well fulfilled. As a reference, the spectrum for the fragment mass region 106–108 is superimposed on all other spectra (dotted line). All spectra for fragment mass splits with $A_b < 114$ or $A_b > 138$ are very similar. The high-energy component starts to rise up for fragment mass splits with A_b around 114–116 (it should be remembered, though, that the mass resolution has a fwhm of 5.0). The

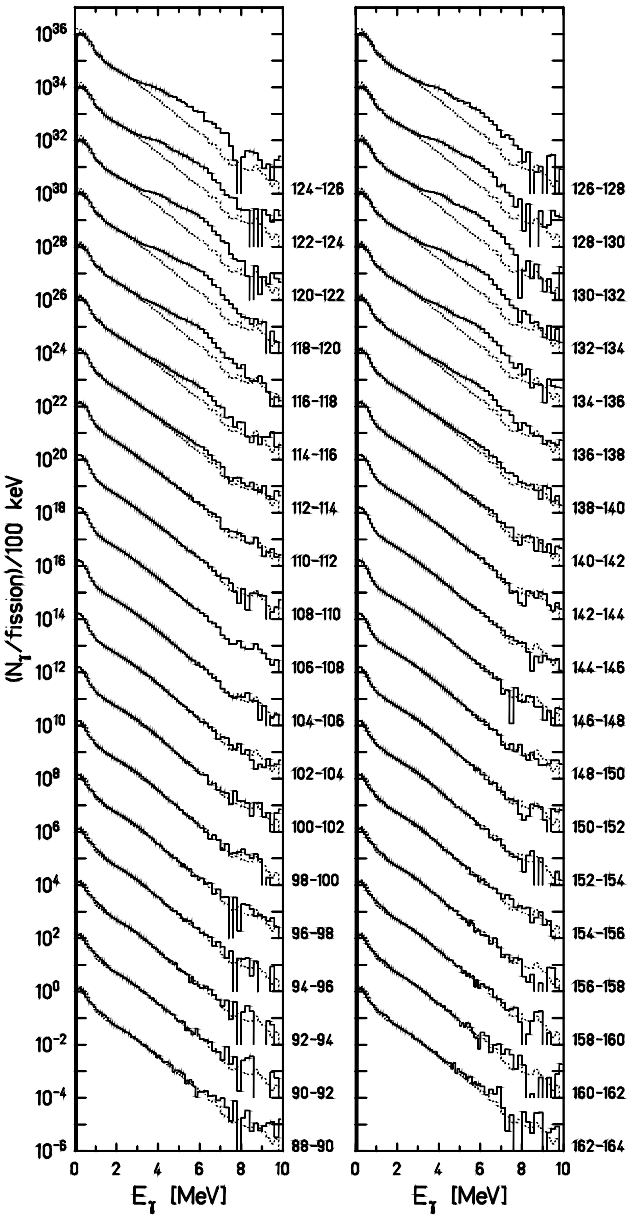

Fig. 5. Normalized γ-energy spectra for different fragment mass splits scaled up by factors of 1, 100, 10 000, etc. The it dotted line shows the spectrum observed for $106 \leq A_b \leq 108$

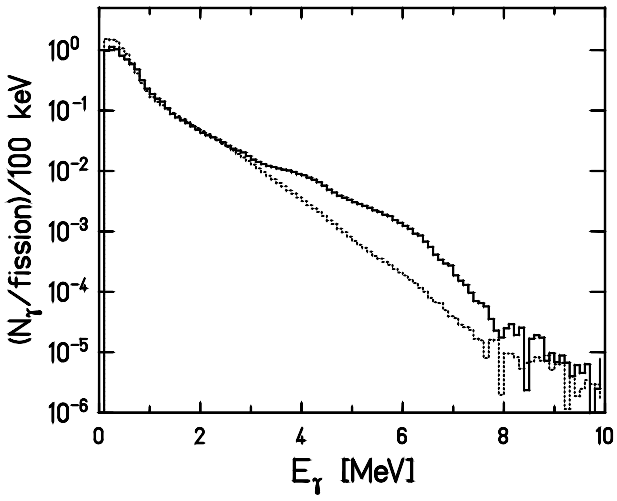

Fig. 6. Normalized γ-energy spectra. Full line: fragment mass splits with $118 \leq A_b \leq 122$ or $130 \leq A_b \leq 134$. Dotted line: fragment mass splits with $106 \leq A_b \leq 110$ or $142 \leq A_b \leq 146$

bump is most pronounced for fragment mass splits with A_b between 120 and 122, or 130 and 132, respectively. For these mass splits, the γ-spectrum seems to be further enhanced by a second, narrower bump centered at approximately 4 MeV. This might be due to transitions in the doubly magic nucleus ^{132}Sn, which has a high-lying first excited state at 4.04 MeV. Roughly 10% of the fission products with mass 132 are ^{132}Sn nuclei [12].

Shape, magnitude, and mass dependence of the high-energy component are in excellent agreement with the previous crystal ball results [1, 2].

In Fig. 6 we show the energy spectrum for the fragment mass region 118–122 (or 130–134), where the high-energy component is largest, together with a typical "ordinary" spectrum for the fragment mass region 106–110 (or 142–146). All events which fulfill the given fragment mass conditions are included, no matter which fragment was detected on which side of the cathode. The γ-bump starts around 3–4 MeV and terminates around 8 MeV. (Note that 8 MeV is approximately the amount of excitation energy taken away by an evaporated neutron). Around E_γ = 6 MeV the enhancement of the γ-spectrum by the γ-bump amounts to almost one order of magnitude.

Gamma-spectra deconvoluted from the response matrix of the crystal ball, as discussed in Sect. 2.3, are shown in Sect. 4.

Figure 7 shows integrals of the γ-spectrum for different energy ranges as a function of the fragment mass A_b. Each channel is normalized according to the number of fissions recorded with the respective mass split. Vertical bars denote statistical errors. At γ-energies below 3 MeV and above 8 MeV, no characteristic fragment mass dependences are visible. The high-energy component obviously starts around 3.5 MeV; between 4 and 8 MeV, its fragment mass distribution has the shape of two overlapping Gaussians centered at 120 and 132, respectively, which sit on top of an almost flat background of statistical γ-rays. Also for extremely asymmetric fragment mass splits, beyond the ratio of 160:92, the γ-spectrum is enhanced between 4 and 8 MeV, though not as dramatically as for mass splits near symmetry.

The distributions displayed in Fig. 7 are not corrected for the absolute detection efficiency. In Fig. 12 of Sect. 4, we show the integral from 3.5 to 8 MeV of the γ-spectrum, deconvoluted from the crystal ball response matrix, as a function of fragment mass. For the deconvolution procedure, the γ-spectrum was symmetrized in the mass dimension, i.e. no distinction was made which fragment was detected on which side of the cathode. Each channel in Fig. 12a was normalized according to the number of fission events recorded with the respective mass split.

The resulting mass dependence of the γ-multiplicity is still smeared out by the finite fragment mass resolution of

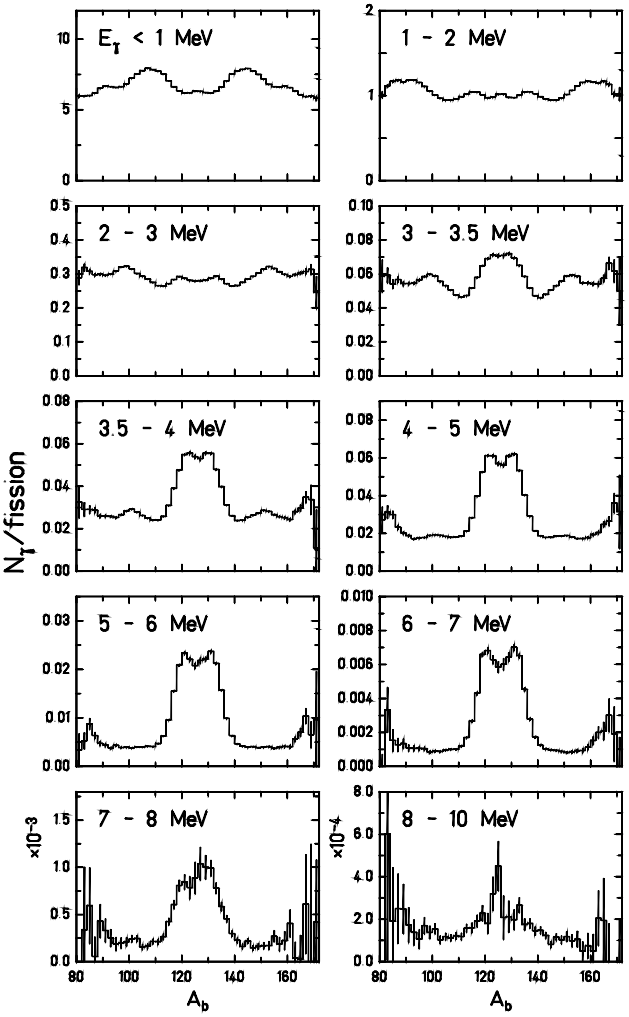

Fig. 7. Normalized integrals of the γ-spectrum over different energy ranges as a function of fragment mass (see text)

5.0. In order to get the parameters of the real mass dependence, we proceeded in the following way: The unnormalized integrals of the deconvoluted γ-spectrum were determined as a function of fragment mass. A background proportional to the measured fragment mass yield, adjusted at the mass region 105–110, was subtracted. The resulting unnormalized fragment mass dependence of the high-energy component was then described by two overlapping Gaussians, and analytically corrected for the mass resolution of 5.0. Moreover, the measured fragment mass spectrum (see fig. 4b) was corrected for mass resolution by an iterative unfolding procedure. Finally, the corrected, unnormalized mass dependence of the high-energy component, described by two overlapping Gaussians, was divided by the unfolded fragment mass spectrum.

As a result, the above analysis yields the mean multiplicity per fission event of bump γ-rays with an energy between 3.5 and 8 MeV as a function of fragment mass. This mass dependence of the γ-multiplicity could again be well described by two symmetric Gaussians, with the parameters:

- centers: A = 120.2 , 131.8
- width (fwhm): ΔA = 6
- height: 0.40 γ/fission
- background of statistical γ-rays: 0.20 γ/fission.

Thus 40% of the fission events with a primary mass split of 132:120 are accompanied by an additional high-energy γ-quant. Assuming the γ-rays to be emitted after neutron evaporation and taking into account the mean neutron multiplicities from [8], the maxima of the distribution correspond to the masses 117 and 131, respectively.

3.2 TKE dependence of the high-energy component

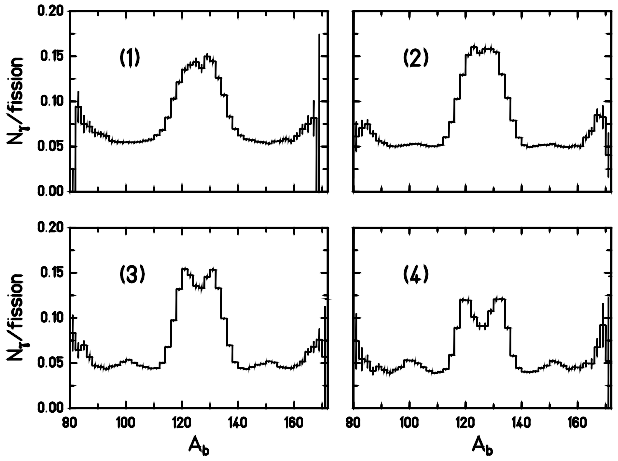

Fig. 8. Normalized integrals of the γ-spectrum from 3.5 to 8 MeV, as functions of fragment mass, for the TKE regions 1 to 4 defined in Fig. 4

Figure 8 shows the integrals of the γ-spectra between 3.5 and 8 MeV as functions of the fragment mass A_b for the four TKE regions defined in Fig. 4. Each channel is normalized according to the number of fission events with the respective mass split and TKE. Both the double hump and the smaller enhancement for extremely asymmetric fragment mass splits are found in all four TKE regions. The mass dependence of the high-energy component is similar in the TKE regions 1 to 3, only between region 3 and region 4 it decreases by a factor of 3/4. On the other hand, the width of the distribution decreases by a factor of 2 between region 1 and region 4 (the TKE-dependence of the experimental mass resolution is negligible in this context).

The rather weak TKE dependence does not support a connection between the high-energy component and the shape of the fragments at the scission point. Judging from the TKE data, it seems more likely that this component is emitted after the equilibration of the fragments, and even after neutron evaporation has taken place. This allegation is also backed by the fact that the upper energy limit of the bump is approximately equal to the energy needed for the evaporation of a neutron and by the findings described in the following subsection.

3.3 Effective velocity and angular distribution of the high-energy component

Two different kinds of information can be derived from the angular distribution of the γ-rays with respect to the fission axis. On the one hand, the angular distribution is Doppler-shifted as a consequence of the motion of the fragments. The magnitude and the sign of the mean Doppler shift of the γ-spectrum depend on the relative contributions of the two fragments, which can thus be deduced. On the other hand, the form of the Doppler-corrected angular distribution is determined by the multipolarities of the transitions which cause the γ-rays.

This information was deduced in the following way: Consider a γ-quant emitted with an energy E' and a polar angle θ' in the rest frame of the emitting nucleus which is moving in positive z-direction. This γ-quant is measured to have the energy E and the polar angle θ in the laboratory system which are given by the relations:

$$E' = (1 - \beta \cdot \cos\theta) \cdot E \tag{3}$$

$$\cos\theta' = \cos\theta - \beta + \beta \cdot \cos^2\theta \tag{4}$$

where β is the velocity of the nucleus in units of c, and only first-order terms in β are kept. Thus the γ-spectrum $Y'(E', \cos\theta')$ in the rest frame of the decaying nucleus is transformed into the laboratory spectrum $Y(E, \cos\theta)$ according to the formula:

$$\begin{aligned} Y(E,\cos\theta) = {} & Y'(E,\cos\theta) \cdot (1 + \beta \cdot \cos\theta) \\ & - \beta \cdot E \cdot \cos\theta \cdot \left.\frac{\partial Y'}{\partial E'}\right|_{E,\cos\theta} \\ & - \beta \cdot (1 - \cos^2\theta) \cdot \left.\frac{\partial Y'}{\partial \cos\theta'}\right|_{E,\cos\theta} \end{aligned} \tag{5}$$

Integration of Y over the energy range $[E_1, E_2]$ and the angular range $[\cos\theta_1 = 0, \cos\theta_2 = 1]$ yields the integral

$$\begin{aligned} I(E_1,E_2,0,1) = {} & \int_{E_1}^{E_2} dE \int_0^1 d\cos\theta \cdot Y'(E,\cos\theta) \\ & -\beta \cdot \left\{ \int_0^1 d\cos\theta \cdot \cos\theta \cdot \left[E \cdot Y'(E,\cos\theta)\right]_{E_1}^{E_2} \right. \\ & \left. - \int_{E_1}^{E_2} dE \cdot Y'(E,\cos\theta = 0) \right\} \end{aligned} \tag{6}$$

If the angular distribution is forward–backward-symmetric in the rest frame of the nucleus, the integral over the angular range $[\cos\theta_1 = -1, \cos\theta_2 = 0]$ differs only by the sign of the Doppler term. Solving equation (5) for Y' and equation (6) for β yields

$$Y'(E,\cos\theta) = \frac{1}{2} \cdot [Y(E,\cos\theta) + Y(E,-\cos\theta)] \tag{7}$$

and

$$\begin{aligned} \beta = {} & [I(E_1,E_2,-1,0) - I(E_1,E_2,0,1)] \\ & \cdot \left\{ \int_0^1 d\cos\theta \cdot \cos\theta \,[E\,(Y(E,\cos\theta) + Y(E,-\cos\theta))]_{E_1}^{E_2} \right. \\ & \left. -2 \cdot \int_{E_1}^{E_2} dE \cdot Y(E,\cos\theta = 0) \right\}^{-1} \end{aligned} \tag{8}$$

The assumptions leading to equations (7) and (8) are well fullfilled: The fragments are slow enough to justify a limitation to first-order terms in β. Moreover, from parity conservation, it is ensured that the partial spectra of the fragments are, in the respective rest frames, forward–backward-symmetric with respect to the fission axis.

In the case of spontaneous fission, there is not only one emitting nucleus, but two fragments moving in opposite directions. Identifying the positive z-axis with the direction of the fragment A_b, Eq. (7) remains valid if Y still denotes the measured γ-spectrum and Y' is interpreted as the average of the angular correlation functions of the two fission products in their respective rest frames. Moreover, an effective velocity $\beta_{\text{eff.}}$ can be assigned to the γ-spectrum, by inserting the total measured spectrum for Y in formula (8). The value of $\beta_{\text{eff.}}$ will vary for different γ-energy regions according to the relative contributions of the two fragments to the spectrum at these γ-energies. The value $\beta_{\text{eff.}}$ must lie between the two fragment velocities, and in the limiting case of all γ-rays coming from the same fragment, must be equal to the velocity of this fragment. Note that the fragment on the source side has, by definition, a negative velocity.

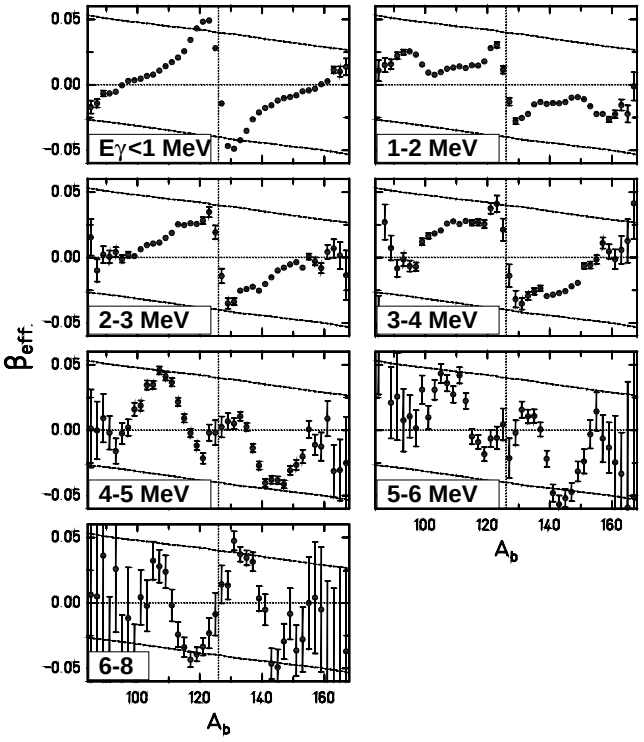

Fig. 9. Effective velocity $\beta_{\text{eff.}}$ as a function of fragment mass for different γ-energy regions, as derived from the Doppler shift of the γ-spectrum (see text, only statistical errors are given). The mass variable A_b refers to the fragment on the backing side. The dashed lines denote the two average fragment velocities.

For the analysis of the angular distribution, our data were corrected for the relative NaI-detector efficiencies (see Sect. 2.3). Figure 9 shows the value of $\beta_{\text{eff.}}$ deduced from our data as a function of fragment mass for different γ-energy regions. The dashed lines are the velocities of the two fragments, calculated from the measured kinetic energies.

The extracted values of $\beta_{\text{eff.}}$ generally lie between the two limits given by the fragment velocities, indicating that the underlying assumptions are well fulfilled — it should be emphasized that $\beta_{\text{eff.}}$ was derived solely from the crystal ball data, the fragment velocities solely from the DIC data. The symmetry around A_b = 126 is also well fulfilled.

Up to γ-energies of 4 MeV, the larger fraction of γ-rays is evidently emitted by the lighter fragment, especially for fragment mass splits near symmetry. The shapes of the distributions correspond to the γ-sawtooths known from literature [15].

Above 4 MeV, the scenario changes for near-symmetric fragment mass splits, whereas for more asymmetric splits, the majority of the γ-rays still come from the lighter fragment. The situation is particularly telling for γ-energies between 6 and 8 MeV, where the relative intensity of the high-energy component reaches its maximum. The $\beta_{\text{eff.}}$ values observed are a clear indication that the high-energy component is emitted predominantly by the heavier fragment, i. e. by fragments with masses close to 132. In fact, by comparing the dependence of the effective velocity $\beta_{\text{eff.}}$ on E_γ for the (symmetrized) mass splits with $142 \leq A \leq 145$ (no γ-bump) and $130 \leq A \leq 134$ (maximal γ-bump), taking into account the corresponding γ-yield ratio, our data are found to be fully consistent with the assumption that the high-energy γ-rays originate from the fully accelerated heavy fragments around A =132.

For the evaluation of the anisotropy of the γ-radiation, Legendre polynomials were fitted to the Doppler-corrected angular distribution of the γ-rays, determined relative to the fission axis. Since our procedure assumes forward–backward symmetry via (7), only even polynomials were considered. Moreover, the coefficients of the fourth and higher orders were compatible with 0 within the statistical errors, so finally the fits were limited to the second-order Legendre polynomial, i. e.

$$Y'(E_\gamma, \cos\theta) = a_0(E_\gamma) \cdot \left(1 + a_2(E_\gamma) \cdot P_2(\cos\theta)\right) \qquad (9)$$

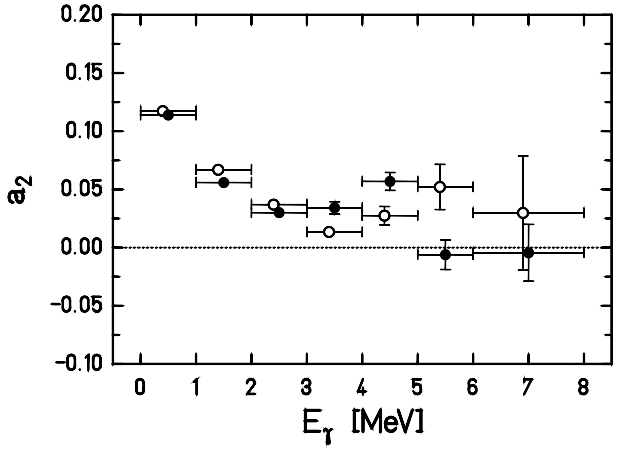

Fig. 10. The correlation coefficients a_2 as a function of γ-energy (see text). Open circles: fragment mass splits with $106 \leq A_b \leq 110$ or $142 \leq A_b \leq 146$. Full circles: fragment mass splits with $118 \leq A_b \leq 122$ or $130 \leq A_b \leq 134$. The horizontal error bars denote the γ-energy regions integrated over, the vertical ones are the statistical errors.

The resulting a_2-coefficients are shown in Fig. 10 as functions of γ-energy for two different fragment mass cuts. (Note that the influence of the finite opening angle of the NaI modules onto a_2 is only a few percent and can therefore be neglected in the following discussion.) The open circles belong to mass splits with $106 \leq A_b \leq 110$ or $142 \leq A_b \leq 146$, where the high-energy component does not appear, the full circles to mass splits with $118 \leq A_b \leq 122$ or $130 \leq A_b \leq 134$, where the bump is most pronounced.

The horizontal error bars denote the γ-energy regions to which the a_2-values belong. The vertical error bars denote the statistical errors only. As we mentioned in Sect. 2.3, the angular distribution at high γ-energies might be affected by γ-n-summing effects. However, while the a_2-values for the more asymmetric mass splits were found to be indeed sensitive to variations in the set of parameters used for the correction, for fragment mass splits near symmetry, where the ratio between real γ and γ-n-summing events was more favourable, the a_2-values stayed qualitatively the same for all reasonable sets of parameters. Therefore, we feel safe to conclude that the angular distribution of the high-energy component between 5 and 8 MeV for near symmetric mass splits is isotropic within the statistical errors, as expected in case the γ-rays are emitted in statistical decay processes occurring e. g. during the cooling phase of the thermally equilibrated fission fragments. In particular, the measured angular distribution does not support an interpretation of the γ-bump as the low-energy component of the giant dipole resonance being shifted down in energy due to a large prolate deformation. The slightly positive a_2-value around 4 MeV might be connected with the additional bump seen in the energy spectrum at this energy.

4 Comparison with CASCADE calculations

Statistical model calculations with the CASCADE code [16] using standard input parameters [17] did not reproduce the observed enhancement of the high-energetic γ-rays connected with the ^{252}Cf fission fragments with masses around symmetry, while good agreement between measured and calculated γ-spectra were obtained for all other mass splits. Therefore, it was speculated in [1] that these γ-rays might be of non-statistical origin. However, our new data clearly show that the bump γ-rays are emitted isotropically and originate from accelerated fragments with (post-neutron) masses around $A \approx 131 \pm 3$, i. e. from nuclei with proton and neutron numbers close to the magic values Z=50 and N=82. This suggests that the observed enhancement in this narrow mass region might be caused by the special structure of these fragments, and that also these γ-rays might be due to the statistical decay of the equilibrated fission products. In fact, in 1988 Budtz-Jørgensen and Knitter [18] deduced the dependence of the level density parameter on the fragment mass from a careful and detailed measurement of the neutron energy spectra and the neutron multiplicities accompanying the spontaneous fission of ^{252}Cf. They found that the level density parameters in the mass region between $A \approx 125$ and $A \approx 135$ are smaller by up to a factor of 3 than those determined by Dilg et al. [17] which had so far been used in statistical model calculations. Using the level density pa-

rameters from [18], Hofman et al. [6] and in particular van der Ploeg [19, 20] have shown that indeed an enhancement of the statistical γ-spectra for γ-energies between 4 and 8 MeV is predicted for mass splits involving fragments around A = 130.

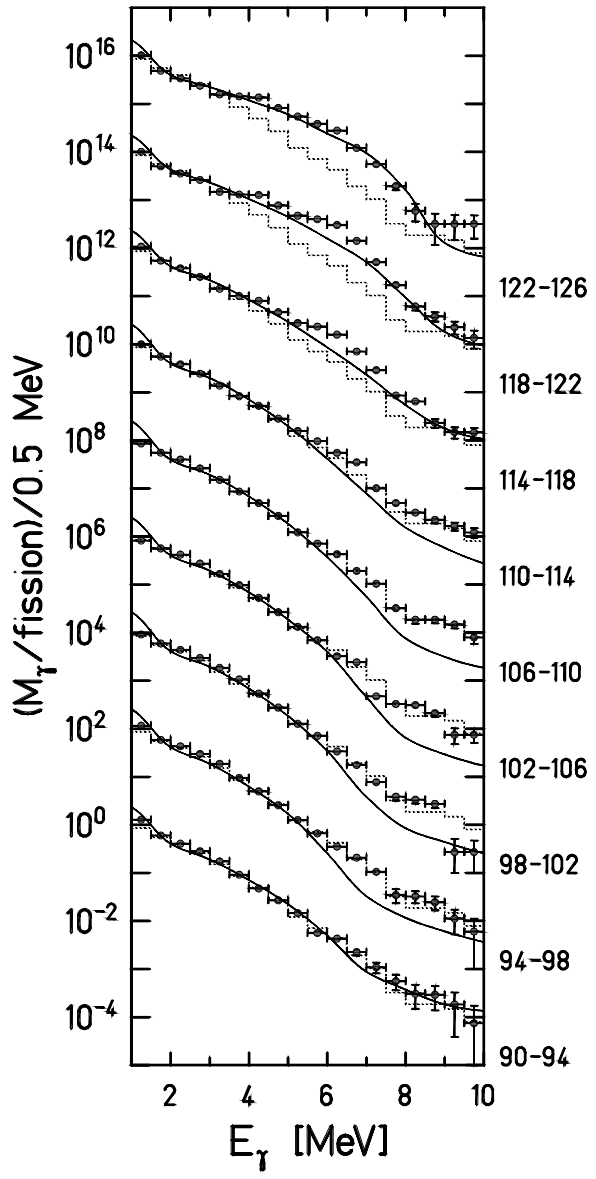

Fig. 11. Comparison of the experimental γ-spectra with CASCADE calculations. Dots: measured, deconvoluted γ-energy spectra for different mass splits (see also text). The spectra are scaled up by factors of 1, 100, 10 000 etc. Dotted lines: reference spectrum ($106 \leq A \leq 110$). Full curves: CASCADE calculations.

In the following we compare our measurements to CASCADE calculations where both the level densities and the initial temperatures were taken from [18]. In Fig. 11 the deconvoluted, mass-symmetrized γ-ray spectra are shown for various mass splits and compared to the corresponding CASCADE predictions without adjusting any further parameter. The experimental γ-spectra displayed in Fig. 11 were obtained by summing over all emission angles and all total kinetic energies as well as over the two equivalent mass splits; they were unfolded from the crystal ball response matrix and then normalized to the number of fission fragments observed for the given mass splits. The mass values given to the right of Fig. 11 correspond to the lighter fragment mass. Obviously, the agreement between the statistical model calculations and the data is remarkably good up to γ-energies of about 7–8 MeV. In particular, the γ-bump observed around symmetric mass splits is well reproduced.

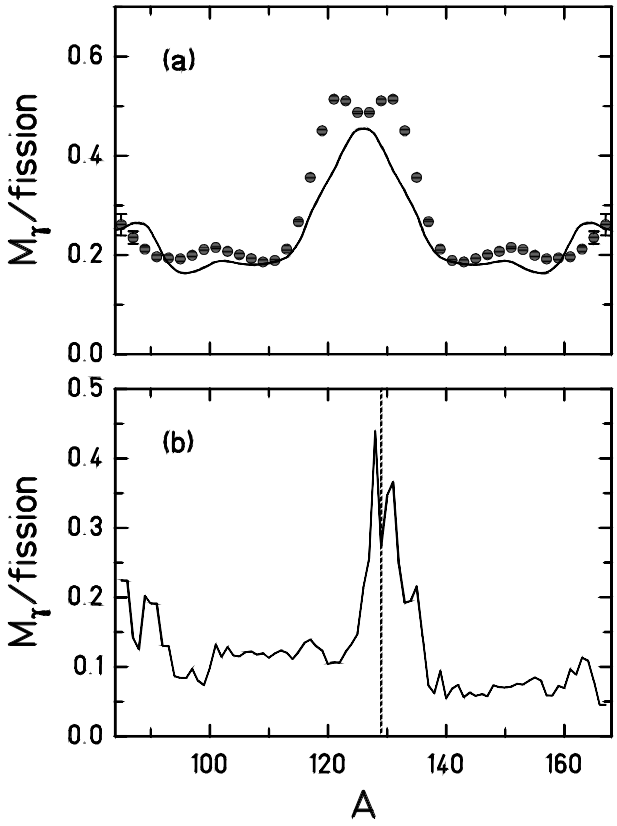

Fig. 12. a Efficiency corrected total number of γ-rays with energies between 3.5 and 8 MeV per fission event as a function of the fragment mass split. Dots: measured values deduced from Fig. 11 (note that these values are not unfolded from the experimental *mass* resolution). Solid curve: CASCADE calculation, folded with the experimental mass resolution. **b** CASCADE calculation of the γ-yield between 3.5 and 8 MeV for the individual fragments as a function of mass

The mass dependence of the calculated γ-ray yield for γ-energies between 3.5 and 8 MeV is displayed in more detail in Fig. 12. In Fig. 12b the calculated yield of γ-rays emitted by an individual fission fragment is shown as a function of the primary mass of the fragment; this yield peaks at A = 128 and A = 131, where the level density parameters deduced in [18] reach a minimum. Note that, assuming a uniform charge distribution, fragments with Z = 50 correspond to A = 128, and that fragments with N = 80 have mass numbers around A = 131. For comparison with our data the calculated γ-multiplicity was symmetrized around A = 126 and folded with the experimental mass resolution, taking into account the fragment mass distribution of ^{252}Cf(sf). As can be seen

in Fig. 12a, the general trend of our data is well reproduced by the statistical CASCADE calculations, although we find – as already shown in our analysis presented in Sect. 3.1 – a slightly more pronounced maximum at the somewhat higher mass of A =131. It must be remembered, though, that the level density parameters were extracted from neutron energy spectra, and thus from a domain of higher excitation energy. For the lower-energy regime where the γ-rays are emitted, the best fit of level density parameters might be slightly different.

Above E_γ =8 MeV the CASCADE calculations lie, for almost all mass splits, below our data. As shown in [19, 20], this energy region is strongly influenced by the details of the initial excitation energies assumed for the fragments — in distinct contrast to the γ-energy region below 8 MeV, which mainly depends on the level densities. Although it seems possible to improve the agreement in the high-energy range by a fine tuning of the excitation energies within the border lines allowed by our present knowledge of this quantity, one should keep in mind that because of the γ-n-summing corrections we had to apply to the data, the evaluated γ-ray yield above 8 MeV might be subject to systematic errors.

5 Summary

Using a position sensitive double ionization chamber with an active solid angle of 60% of 4π, together with a 4π γ-array built of 162 NaI detectors (crystal ball), the high-energy γ-spectra accompanying the spontaneous fission of ^{252}Cf have been measured as a function of the mass split and the total kinetic energy. We could show that the previously observed enhancement of the γ-ray spectra at γ-energies between 4 and 8 MeV [1] are caused by γ-rays emitted from a group of fully accelerated fragments with an average mass number of A = 131 (after neutron emission) and a fwhm of ΔA = 6. At A = 131 the total probability per fission event for the emission of a γ-quant between 3.5 and 8 MeV reaches 60% (as compared to 20% for asymmetric mass splits), and the angular distribution of these γ-rays with respect to the fission axis was found to be isotropic within the accuracy of the experiment. The dependence of the enhancement on the total kinetic energy of the fission products is weak.

These findings could be reproduced in their main features by statistical model calculations using the CASCADE code and realistic input values for the level densities and initial excitation energies of the fragments. It turns out that in the energy domain below the neutron evaporation threshold of about 8 MeV, the level density actually determines the shape of the γ-spectra [19, 20], and that the strong enhancement observed for fission fragments around A=131 is explained by the strongly reduced level densities in the vicinity of the shell closures at Z = 50 and N = 82.

Our conclusion that the enhancement is due to properties of the equilibrated fission fragments rather than to effects connected with the fission process itself, is also borne out by the results of [3]. Here, for different fusion-fission reactions an increase in the γ-ray intensity between 3 and 9 MeV has been observed as well for fission events with one fragment near A = 131.

This work was partly supported by the BMBF under contract nr. 06HD525I, 06DA461, and 06TU669.

References

1. Glässel P., Schmid-Fabian R., Schwalm D., Habs D., and v. Helmolt H. U., Nucl. Phys. **A502**, 315c (1989)
2. Wiswesser A., Diploma Thesis, MPI für Kernphysik, Heidelberg (1992)
3. Fitzgerald J. B., Habs D., Heller F., Reiter P., Schwalm D., Thirolf P., Wiswesser A., to be published in Z. Phys.
4. Brosa U., Großmann S., and Müller A., Phys. Reports **197**, 167 (1990)
5. Pomorski K., Richert J., Bartel J., Dietrich K., Z. Phys. **A339**, 155 (1993)
6. Hofman D. J., Back B. B., Montoya C. P., Schadmand S., Varma R., Paul P., Phys. Rev. C **47**, 1103 (1993)
7. Metag V., Lecture Notes in Physics **178**, 163 (1983)
8. Düring I., Thesis, TU Dresden (1993)
9. Schmitt H. W., Kiker W. E., and Williams C. W., Phys. Rev. **137**, B837 (1965)
10. Hotzel A., Diploma Thesis, MPI für Kernphysik, Heidelberg (1994)
11. Lederer C. M. and Shirley V., Table of Isotopes, Wiley, New York, 7. edt. (1978)
12. Wahl A. C., At. Data and Nucl. Data tables **39**, 1 (1988)
13. Reiter P., Diploma Thesis, MPI für Kernphysik, Heidelberg (1989)
14. Thirolf P., Thesis, Universität Heidelberg (1992)
15. Jonansson S. A. E., Nucl. Phys. **60**, 378 (1964)
16. Pühlhofer F., Nucl. Phys. **A280**, 267 (1977)
17. Dilg W., Schantl W., Vonach H., and Uhl M, Nucl. Phys. **A217**, 269 (1973)
18. Budtz-Jørgensen C. and Knitter H. H., Nucl. Phys. **A490**, 307 (1988)
19. van der Ploeg H., PHD Thesis, Rijksuniversiteit Groningen (1995)
20. van der Ploeg H., Bacelar J. C. S., Buda A, Laurens C. R., van der Woude A., Gaardhøje J. J., Zelazny Z., van't Hof G., and Kalantar-Nayestanaki N., Phys. Rev. **C52**, 1915 (1995)

This article was processed by the author using the LaTeX style file *pljour2* from Springer-Verlag.